ISSN: 2447-3359

REVISTA DE GEOCIÊNCIAS DO NORDESTE

Northeast Geosciences Journal

v. 10, nº 2 (2024)

https://doi.org/10.21680/2447-3359.2024v10n2ID36277

Evaluation of the positional accuracy of terrestrial laser scanner using a perpendiculars 3D plans system

Avaliação da precisão posicional de laser scanner terrestre utilizando um sistema de planos perpendiculares 3D

Paulo Augusto Ferreira Borges[1]; Edvaldo Simões da Fonseca Junior[2]; William Rodrigo Dal Poz[3]

[1] Federal Institute of Education, Science and Technology of Southern Minas Gerais, Inconfidentes Campus, Inconfidentes/MG, Brazil. Email: paulo.borges@ifsuldeminas.edu.br.
ORCID: https://orcid.org/0000-0002-4792-8637.

[2] University of São Paulo, Polytechnic School (EPUSP), Department of Transportation Engineering, São Paulo/SP, Brazil. Email: edvaldoj@usp.br.
ORCID: https://orcid.org/0000-0002-4910-9109.

[3] Federal University of Viçosa, Department of Civil Engineering, Viçosa/MG, Brazil. Email: william.dalpoz@ufv.br.
ORCID: https://orcid.org/0000-0001-9532-3643.

Abstract: Terrestrial Laser Scanner (TLS) is routinely used in different measurement applications in precision engineering. Due to wear, aging, and restrictions on the internal components of a TLS, systematic errors arise that impair the calibration parameters prescribed by the manufacturer, requiring a new process of deleting additional TLS configurations. In this case, self-calibration is used, which involves the implementation of fixed targets, requiring prior and thorough preparation. Thus, there is an interest in easy-to-use and applied measurement methodologies, which allow quantifying and evaluating the quality and precision of a TLS. This article proposes a method for the calibration of TLS with a three-dimensional system of perpendicular planes, where the 3D accuracy of the TLS can be obtained from the point cloud of different planes. The results were achieved with confidence and trust. For scanning distances of 1, 3, and 5 meters in resolutions of 1/2, 1/5, and 1/8, the RMS values did not exceed 2 mm for the X and Y axes and exceeded 2 mm for the Z axis. For distances of 10 meters and the same resolutions, the RMS values for the X and Y axes were above 2 mm, while for the Z axis, RMS values of 2.88 mm, 3.79 mm, and 4.73 mm were obtained in the above resolutions. Note the performance degradation of TLS for scanning distances of 15, 20, and 25 meters, emphasizing the 1/4 resolution, which presented a lower RMS.

Keywords: Terrestrial laser scanner; Cloud of points; Systematic Errors; Calibration; Precision; Accuracy.

Resumo: Laser Scanner Terrestre (LST) são utilizados rotineiramente em diferentes aplicações de medição na engenharia de precisão. Devido ao desgaste, envelhecimento e deterioração dos componentes internos de um LST, surgem erros sistemáticos que afetam os parâmetros de calibração estabelecidos pelo fabricante, exigindo-se um novo processo de calibração dos parâmetros adicionais do LST. Neste caso, emprega-se a autocalibração, que demanda implantação de alvos fixos, exigindo um preparo prévio e minucioso. Assim, surge o interesse por metodologias de aferição de fácil utilização e manuseio, que permita quantificar e avaliar a qualidade e a acurácia de um LST. Este artigo apresenta a proposta de um método de aferição de LST com um sistema tridimensional de planos perpendiculares, onde a partir da nuvem de pontos dos diferentes planos pode-se obter a acurácia 3D do LST. Os resultados alcançados se mostraram satisfatórios e confiáveis. Para distâncias de varredura de 1, 3 e 5 metros nas resoluções de 1/2, 1/5 e 1/8 os valores RMS não ultrapassaram 2 mm para os eixos X e Y e ligeiramente superiores a 2 mm no eixo Z. Na distância de varredura de 10 metros e mesmas resoluções, os valores RMS para os eixos X e Y, ficaram acima de 2 mm, já para o eixo Z obteve-se RMS de 2,88 mm, 3,79 mm e 4,73 mm nas resoluções citadas, respectivamente. Observou-se a degradação do desempenho do LST para as distâncias de varredura de 15, 20 e 25 metros, com destaque para a resolução de 1/4 que apresentou um RMS menor.

Palavras-chave: Laser scanner terrestre; Nuvem de pontos; Erros Sistemáticos; Calibração; Precisão; Acurácia.

Received: 14/05/2024 Accepted: 05/07/2024; Published: 22/10/2024

1. Introduction

Terrestrial Laser Scanners (TLS) have proven to be a highly accurate and efficient method for acquiring three-dimensional information from objects with high data density. The characteristics and capabilities of modern TLS systems have opened new fields of application to the market, from geosciences to the film industry (CHOW, LICHTI, and TESKEY, 2010). The application of TLS in geosciences has increased rapidly in the last two decades, including geology, seismology, natural hazards, geomorphology, and glaciology (TELLING et al., 2017).

This equipment stands out due to the high accuracy obtained in surveys, being able to reach precision levels in the hundredth of a millimeter, a precision observed in industrial trackers and articulated arms frequently used for inspection and reverse engineering design applications in different industrial areas such as aerospace, defense, automotive and renewable energy. It is also worth mentioning that reflectors do not need to collect distances to objects, in addition to the high resolution, generating dense point clouds with rates reaching up to 2 million points/s (FARO, 2022).

To generate three-dimensional coordinates (x, y, z) of points on a surface, TLS emits laser pulses with the help of a scanning mirror. The laser pulse hits the object, and part of the energy returns to the system, allowing the distance to be calculated.

When the distance is determined through the time interval between the emission and the return of the pulse, it is called direct time-of-flight measurement (SHAN; TOTH, 2017). The FMCW (Frequency-Modulated Continuous Wave) method is also mentioned, and it was initially designed for use in radars. According to Hancock (1999), this method is based on the modulation of the amplitude of an emitted signal through frequency variation. The emitted signal is modulated by a sinusoidal wave with a variable frequency that "mixes" with the reflected frequency. The mixed frequency passes through a low-pass filter, and thus, the distance is obtained by measuring the resulting beat frequency. Currently, most commercial TLSs use the AMCW (Amplitude-Modulated Continuous Wave) method, which modulates the electromagnetic energy emitted from a sinusoidal wave at a given frequency. This is a phase comparison method for measuring the phase shift between the emitted and returned waves.

The level of accuracy of a TLS is linked to the alignment of the internal optical-mechanical components or the calibration parameters that compensate for systematic errors. These parameters are calculated a priori by the manufacturer, who calibrates the equipment before shipping it to the end user. Over time, due to wear, aging, temperature variations, and consequent deterioration of the TLS, the relative position of its internal components changes, resulting in systematic errors that exceed the accuracy listed in the specifications, and the equipment must undergo regular calibrations to update the calibration parameters (QIAO; BUTT, 2023).

Telling et al. (2017) highlight the importance of periodic (annual) maintenance of TLSs, including verification and calibration for application in geosciences, since in these cases, TLS systems are regularly transported and installed in rough terrain and more adverse environments. Although TLSs are precise instruments, they present inevitable measurement errors. These errors mainly come from distortions in the movement mechanisms, errors in the measuring diode, processing errors in the internal software, and other errors caused by dynamic effects and environmental conditions (QIANG; WEI, 2009).

Among the different sources of errors, the following are cited (BOEHLER, BORDAS; MARBS, 2003): instrumental errors (diameter of the laser beam, resolution, edge effect, linear error, angular error, and errors in the axis systems); errors related to the shape and nature of the scanned objects (surface reflectance with the occurrence of multipath); errors caused by the environmental conditions of the scanning site (temperature, atmospheric conditions – presence of fog or dust, radiation interference).

Calibration results with different TLS's and varied methodologies can be found in contributions from several authors, such as Qiao and Butt (2023); Shi, Muralikrishnan and Sawyer (2020); Zhou et al. (2020); Holst et al. (2016); Soudarissanane et al. (2011), Reshetyuk (2010), Kaasalainen et al. (2009), Kersten, Sternberg and Mechelke (2005); Boehler, Bordas and Marbs (2003).

Some studies presented by Lichti (2007, 2008, and 2010) and Chow, Lichti, and Teskey (2010) proposed the modeling of systematic errors using a self-calibration obtained from the collection of redundant observations on several fixed targets, positioning the instrument in different stations. The model variables comprised of the scanner position j, the angular orientation elements, the target parameters, and the coefficients of systematic errors were called additional parameters, estimated from the observations by applying an adjustment by the Least Squares Method (LSM). The advantages of using the self-calibration of TLS include the optimization of the estimation of all the model variables without the need for special equipment or prior knowledge of the coordinates of the targets used. In this case, only one room with several marked targets is used, which will be scanned from different stations.

Other approaches to TLS self-calibration are presented with some variations. Reshetyuk (2006) proposed using a mathematical model in which the coordinates of the targets in the external system are determined independently from a total station whose values, once known, become inputs to the model. In this proposal, the coordinates of the scanner position are chosen from the use of a total station or are estimated from the adjustment by LSM.

Medić, Kuhlmann, and Holst (2021) analyzed different strategies for TLS calibration, proposing an analysis of the calibration results performed by the manufacturer, with two calibrations performed by the user that used fixed targets and known control points. The results demonstrated that user-performed calibrations can replace factory calibration if a comprehensive list of calibration parameters is used, reducing maintenance costs and ensuring the accuracy required for end-user applications.

Qiao and Butt (2023) proposed an autonomous calibration algorithm for TLS, based on the use of plane correction, easily found in urban environments and which does not require prior manual preparation. The scanner calibration parameters are estimated and updated by minimizing the average distances between planes based on a point cloud comparison technique called M3C2. Unlike approaches based on targets or control points, only medium-resolution plane scan data were required. The study used two high-precision TLSs, Leica RTC360 and Z+F Imager 5016, and the results achieved were consistent with target-based calibration techniques. Ten calibration parameters were calculated from a geometric error model developed by the US National Institute of Standards and Technology (NIST), and the results estimated by the proposed algorithm showed variations within ±3 sigma compared to target calibration but with more minor standard deviations.

The different calibration approaches described here show the importance of defining and implementing methodologies that allow quantifying and evaluating the quality and accuracy of terrestrial laser scanner systems and the other errors inherent to the equipment or the measurement process, aiming at certifying them, attesting or not their compliance with the nominal accuracy defined by the manufacturers. This article presents the results of the proposal of a methodology for evaluating the three-dimensional accuracy of terrestrial laser scanners using a steel part with three flat and perpendicular faces, forming a system of three-dimensional axes (x, y, z). By defining the reference system of the point cloud coinciding with the intersection of the three planes, it is possible to evaluate the values of the standard deviations obtained for the three axes (σx, σy, and σz) calculated from a dense cloud of points for each flat face.

2. Method

The flowchart in Figure 1 illustrates the steps for executing the work and summarizes the methodology used, including part calibration, scene scanning, data processing, and analysis of results.

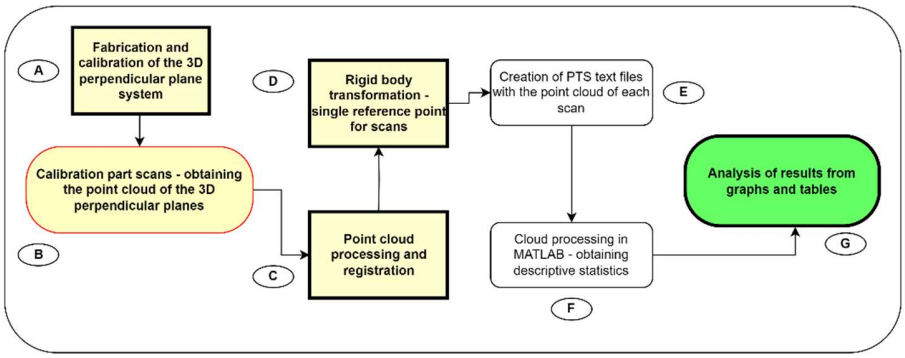

Figure 1 – Flowchart with the data collection and processing methodology.
Source: Authors (2024)

2.1. Fabrication and calibration of the 3D perpendicular plane system

To implement this method, a three-dimensional steel part was constructed consisting of three flat faces perpendicular to each other, with dimensions of 15.875mmx500.000mmx500.000mm, as illustrated in Figure 2.

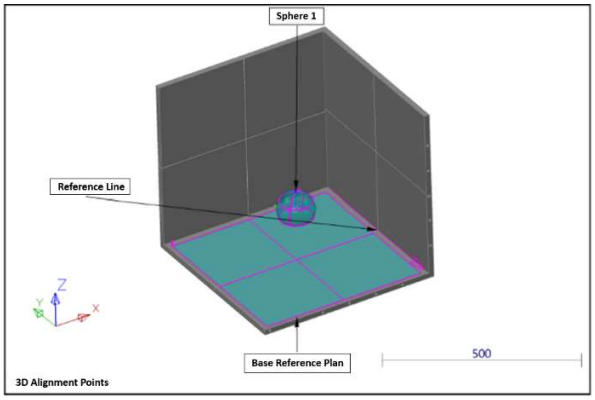

Figure 2 – Diagram showing the three perpendicular faces of the three-dimensional part manufactured for TLS measurement.
Source: Authors (2024).

In machining, planar precision is guaranteed in the order of one-hundredth of a millimeter. The assembly of the three flat faces was carried out to define three perpendicular planes, which were used to determine the three-dimensional error (axes X, Y, and Z) of a TLS. Even though it is a high-precision machining process that follows strict quality control standards, it has become convenient to calibrate the 3D part using equipment with precision that is more significant than a TLS's accuracy level. Therefore, a portable measuring arm, the Homer Absolute model, manufactured by Hexagon Metrology, was used in this process. This procedure was carried out by a company specializing in measuring products and assembly and inspection devices. The purpose of the calibration was to determine the distance from each plane to the center of a polyacetal sphere with a nominal diameter of 100 mm, positioned in the center of the part that defines the horizontal plane (Z axis), as well as to evaluate the perpendicularity between the planes, as illustrated in Figure 3. Table 1 shows the precision specifications of the equipment used:

Table 1 – Technical specifications of the portable measuring arm.

Model	Measuring Range	The repetitiveness of the palpation point	Volumetric Accuracy	Arm Weight (including base)
7125	2.5 m (8.2 ft)	0.050 mm (0.0020 in)	0.069 mm³ (0,0027 in)	7.9 kg (17.42 lb)

Source: Authors (2024).

The equipment has an accuracy of five-hundredths of a millimeter, presenting much higher precision than TLS equipment.

a)  b) 

Figure 3 – a) Professional performing measurement services on the 3D part manufactured for TLS calibration. b) The piece is prepared for sweeping after being painted white.
Source: Authors (2024).

After the calibration process, the nominal distances between the sphere's center and each face were determined by obtaining the $\Delta X, \Delta Y$ and ΔZ reference values. The perpendicularity between the axes was also determined to ensure that the variation in distance from each axis to the center of the sphere remains constant with precision to the hundredth of a millimeter. The values obtained after calibration are presented in Tables 2 to 5 below.

Table 2 – Determination of the reference sphere's nominal diameter (mm).

		Superior Tolerance.	Lower Tolerance	Nominal	Measured	Standard Deviation
Diameter		0.100	-0.100	100.000	100,024	0,024
Center	**X**	0.100	-0.100	0.000	0.000	0.000
	Y	0.100	-0.100	0.000	0.000	0.000
	Z	0.100	-0.100	0.000	0.000	0.000

Source: Authors (2024).
Number of points captured: 5

Table 3 – Determination of the nominal distance from the sphere's center to the Z plane.

Reference - Geometric Alignment PLP 1 (Values in mm)						
		Superior Tolerance.	**Lower Tolerance**	**Nominal**	**Measured**	**Standard Deviation**
Point A1	**Z**	0.200	-0.200	-147.690	-147.692	0.002
Point A2	**Z**	0.200	-0.200	-147.690	-147.692	0.002
Point A3	**Z**	0.200	-0.200	-147.690	-147.692	0.002
Point A4	**Z**	0.200	-0.200	-147.690	-147.692	0.002

Source: Authors (2024).
Reference: PLP 1 (Principal Plane 1 used in the initial alignment of the robotic arm).

Table 4 – Determination of the nominal distance from the sphere's center to the Y plane and the angular deviation from the Y plane to the Z plane.

The angle between Z Plane / Y Plane – Reference: Base Plane Ref. (Z Plane)					
	Superior Tolerance.	**Lower Tolerance**	**Nominal**	**Measured**	**Standard Deviation**
Angle	0.100º	-0.100º	90.000º	89.965º	-0.035º
Reference - Geometric Alignment Plane Z (Values in mm)					
	Superior Tolerance.	**Lower Tolerance**	**Nominal**	**Measured**	**Standard Deviation**

Point B1	**Y**	0.200	-0.200	234.170	234.350	0.180
Point B2	**Y**	0.200	-0.200	234.170	234.077	-0.093
Point B3	**Y**	0.200	-0.200	234.170	234.088	-0.082
Point B4	**Y**	0.200	-0.200	234.170	234.357	0.187
Point B5	**Y**	0.200	-0.200	234.170	234.219	0.049

Source: Authors (2024).

Table 5: Determination of the nominal distance from the sphere's center to the X plane and the angular deviation from the X plane to the Z plane.

The angle between Z Plane / X Plane – Reference: Base Plane Ref. (Z Plane)					
	Superior Tolerance.	**Lower Tolerance**	**Nominal**	**Measured**	**Standard Deviation**
Angle	0.100º	-0.100º	90.000º	89.988º	-0.012º
Reference - Geometric Alignment Plane Z (Values in mm)					
	Superior Tolerance.	**Lower Tolerance**	**Nominal**	**Measured**	**Standard Deviation**
Point C1 **X**	0.200	-0.200	235.050	234.947	-0.103
Point C2 **X**	0.200	-0.200	235.050	234.851	-0.199
Point C3 **X**	0.200	-0.200	235.050	235.213	0.163
Point C4 **X**	0.200	-0.200	235.050	235.118	0.068
Point C5 **X**	0.200	-0.200	235.050	235.032	-0.018

Source: Authors (2024).

Figures 4a, 4 b and 4c show the positions of the measured points A1 to A4, B1 to B5, and C1 to C5, respectively.

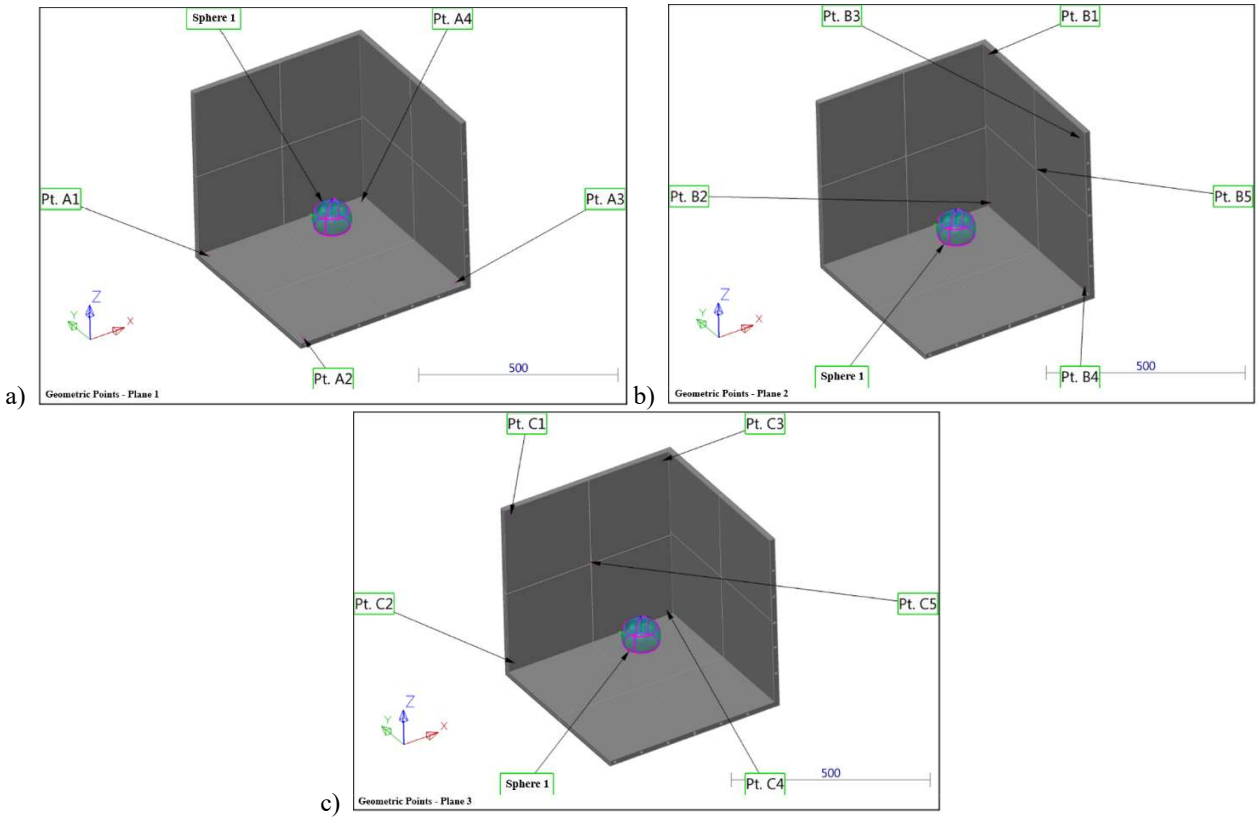

Figure 4 – a) Measured points A1 to A4 on Plane 1; b) Measured points B1 to B5 on Plane 2; and c) Measured points C1 to C5 on Plane 3.
Source: Authors (2024).

Table 2 shows the sphere's nominal diameter and standard deviation, which are necessary for analyzing the scanning distances from the sphere's center to the three perpendicular planes. Tables 3 to 5 show the nominal distances between the sphere's center and each perpendicular plane, Z, Y, and X, respectively, to ensure perpendicularity between them.

After calibrating the plane system and ensuring perpendicularity between the axes with errors lower than the precision of a TLS, the part was scanned to obtain the point cloud on each flat face.

2.2. Data collection and processing methodology

An old TLS, purchased in 2008 and frequently used, model Faro Photon 80 (FS80), was calibrated to evaluate the proposed methodology. According to the manufacturer, the technical specifications of the TLS FS80 guarantee a standard error of $\pm 2mm$ for measurements at distances of up to 25 meters and a horizontal and vertical angular resolution of $\pm 0{,}009°$.

For the three-dimensional scanning process of the calibration part, seven different distances were defined for the positioning of the TLS to be calibrated: 1, 3, 5, 10, 15, 20, and 25 meters. For distances of 1 to 10 meters, three scans were performed with the TLS FS80, configuring different resolutions: 1/2, 1/5, and 1/8 of the maximum resolution of the equipment, which is 120,000 points per second. Due to the size of the calibration part, it was decided to perform the scan with a maximum resolution of 1/1, in addition to the resolutions of 1/2 and 1/4 for the distances of 15, 20, and 25 meters, also changing the positioning of the calibration part, aiming to minimize the influence of the angle of incidence of the laser beam on the horizontal plane of the part, corresponding to the z-axis, as illustrated in Figure 5:

a)  b) 

Figure 5 – a) horizontal positioning for 1 to 10 meters scans. b) 45° positioning for 15, 20, and 25 meters scans. Source: Authors (2024).

Once the scan is performed, the intersection between the three TLS axes is used as a reference point to determine the coordinates of each vertex in the point cloud (Figure 6). The X, Y, and Z coordinates are set to zero for this reference point.

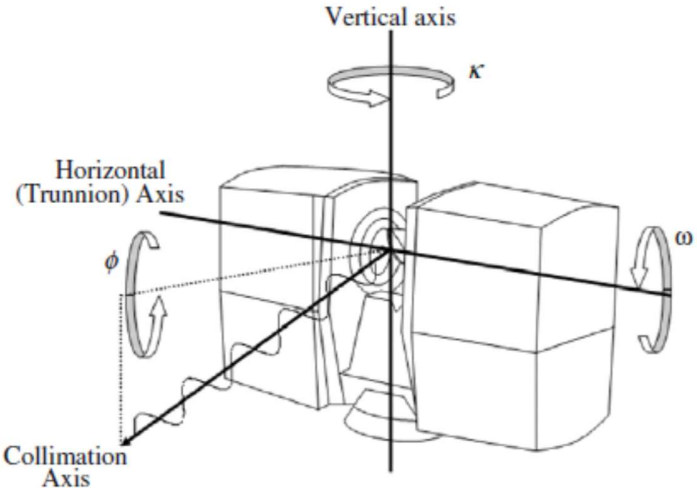

Figure 6 – TLS axes and orientation angles. Source: Lichti (2010).

To facilitate the calibration process, it was decided to transfer the reference point of each scan to a common point, in this case, the intersection of the three flat faces of the calibration part, adjusting each face of the part to its respective reference plane in the new x, y, and z axis system. This process consists of a rigid body transformation with three rotations and three translations, without scale, and was performed in the Faro Scene processing and registration software Version 4.8.4.26611. In this way, the point cloud of each face of the part now presents coordinates close to its origin axis, that is, to the zero value. For this, the automatic plane recognition and adjustment tool was used. In this process, a polygon was defined on each flat face of the calibration part, from which the X, Y, and Z planes were determined in the point cloud. Then, the three reference planes (Figure 7) were defined based on the theoretical average values for positioning the point cloud from the new reference.

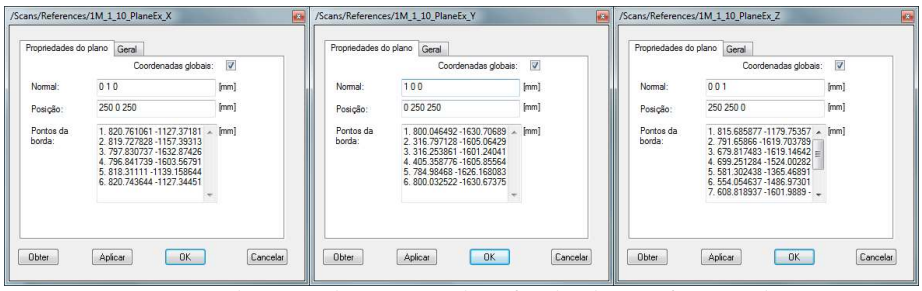

Figure 7 – Theoretical average values for the three reference planes.
Source: Faro Scene Software Version 4.8.4.26611.

Figure 8 illustrates the results of this process for one of the TLS scans.

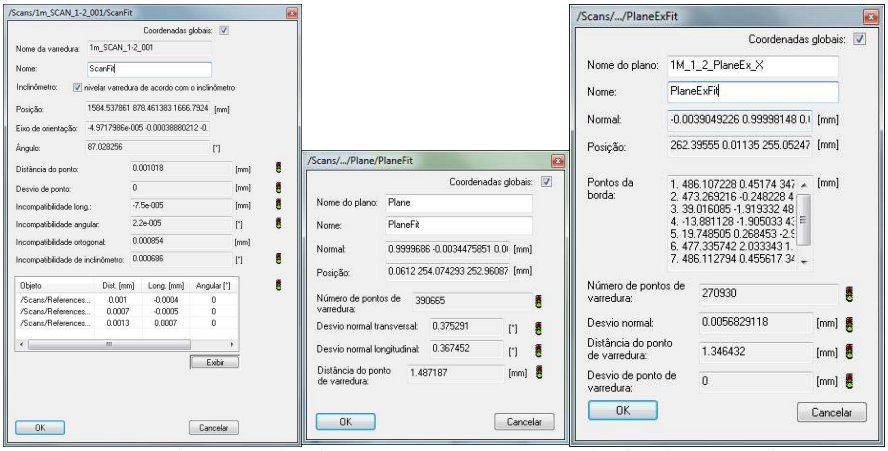

Figure 8 – The point cloud registration process results for the new reference.
Source: Faro Scene Software Version 4.8.4.26611.

The standard deviation of the normal, which is determined using the preliminary results of the adjustment, allows us to indicate whether a selected area is as flat as it should be. A high standard deviation indicates that there may be a wave or other objects in the chosen plane. The Faro Scene software divides this standard deviation into transverse and longitudinal. The quality of this criterion will indicate adequate values when it is less than 1.15° and unacceptable values when it is more significant than 2.29°. Observing Figure 8 on the right, the average distance of 1.346432 mm from the scanning points to the plane stands out and is an excellent indicator for measuring noise. There is also a low error between the theoretical plane and the average plane generated by the point cloud, called normal deviation, with a value of 0.005658 mm. This proves the quality of manufacturing the perpendicular plane system used in the measurement.

When examining a symmetric or approximately symmetric sampling distribution, it is noted that they are generally more frequent near a central value and rarer when moving away from it. Obtaining this central value is of utmost importance in sample surveys. Therefore, the arithmetic mean, median, and mode values were calculated. The sample variance, standard deviation, maximum, minimum, kurtosis, asymmetry, amplitude, and RMS were calculated to analyze the variations around the central measurement.

To eliminate possible gross errors in each sample, the robust estimation algorithm called the Danish method was adopted as a criterion for rejecting possible atypical observations (outliers), which is characterized by better detection of gross errors and rapid convergence (JORGENSEN et al., 1985; KUBIK; WENG; FREDERIKSEN, 1985, apud RESHETYUK, 2006). This algorithm calculates weights for each of the observations from Equation 1 below.

$$P_j = \begin{cases} 1 \; se \; |v_j| < K \cdot \sigma_{v_j} \\ \exp\left(-\frac{v_j^2}{K \cdot \sigma_{v_j}^2}\right) se \; |v_j| \geq K \cdot \sigma_{v_j} \end{cases} \quad (1)$$

Where v_j and σ_{v_j} are the residuals (observed values for each plane) of the j observation and its respective standard deviation, calculated from the entire sample.

Reshetyuk (2006) defines the constant K with the value 3, following practical criteria for identifying outliers. After calculating the P_j matrix, if the values obtained are all equal to 1, there is an indication that no outlier was detected; otherwise, the observations that did not meet the criterion in the first iteration are eliminated, and a new calculation of the statistics is performed.

Since this is an iterative process, the initial calculation of the mean and standard deviation to be used in the first detection of outliers is done directly with the original data, so very discrepant data may contaminate the values of the initial descriptive statistics. Thus, aiming at a quick convergence, before starting the iteration using the Danish method, an initial filtering of the data was done, where, depending on the number of samples of each point cloud on the respective axes, the value k of the number of sigma necessary for only one value of the sample to be outside the interval was calculated, this being the initial value used (only once), replacing the value $k = 3$. The first criterion for rejecting observed values L_i, statistics were calculated by eliminating observations that presented the following values around the mean $\bar{\mu}$: $L_i < \bar{\mu} - k * \sigma_{Li}$ ou $L_i > \bar{\mu} + k * \sigma_{Li}$, where σ_{Li} corresponds to the standard deviation value obtained for the entire sample (total number of observations).

Table 6 presents the values for the quantity k of sigma used in the first filtering, calculated as a function of the number of samples in each point cloud.

Table 6 – Values of k correspond to the total number of each sample.

Resolution	Distances (m)	Std. Deviation X (mm)	Std. Deviation Y (mm)	Std. Deviation Z (mm)	X samples	Y samples	Z samples
1:1	15	4.08	4.10	3.53	22548	25044	2512
	20	3.75	3.95	3.28	5787	13150	994
	25	3.86	3.83	2.82	9088	7931	215
1:2	1	4.70	4.60	4.71	401748	248205	413131
	3	4.44	4.41	4.32	111932	93065	64354
	5	4.25	4.22	4.03	47535	42516	18313
	10	3.95	3.93	3.49	13101	11936	2173
	15	3.76	3.75	3.15	6040	5803	633
	20	3.61	3.60	2.68	3344	3254	141
	25	3.50	3.48	2.22	2237	2044	39
1:5	1	4.31	4.21	4.33	63827	40131	67866
	3	4.02	3.98	3.88	17466	14904	9894
	5	3.81	3.79	3.57	7425	6811	2862
	10	3.49	3.45	2.60	2173	1808	112
1:8	1	4.10	3.99	4.11	24610	15369	25909
	3	3.79	3.74	3.64	6780	5681	3718
	5	3.58	3.54	3.30	2953	2585	1049
	10	3.22	3.19	1.94	814	733	20

Source: Authors (2024).

Next, with the sample data after the first filtering, the Danish method was applied iteratively, recalculating the descriptive statistics after each iteration and performing the rejection criterion analysis until no outliers were detected.

To assess the normality of the data, standard distribution curves and frequency histograms were generated, as well as quantile-quantile plots or q-q plot graphs for all scans. Observing the number of points in each point cloud through Table 6, a vast number of samples can be observed, which made it impossible to apply statistical tests such as the Shapiro-Wilk

test since the sample size must be between 3 and 5000 points. Other statistical tests were evaluated using MATLAB software and the "nortest" package in R software, such as the Anderson-Darling, Jarque-Bera Robust, and Lilliefors tests. However, for all of them, the calculated statistics presented a very small p-value due to the large sample size, making the application unfeasible.

According to Miot (2016), normality analyses based on Q-Q plot diagrams become reliable for large samples (> 5,000 units) when normality tests significantly inflate the type II error (causing loss of sensitivity). The author points out that several statistical tests can be applied to verify the normality of data based on different assumptions and algorithms, where all of them assume the hypothesis of data normality (H_0) based on the adoption of a $p - value > 0.05$, so that there is adherence to the normality parameters. A detailed study with considerations on p-values linked to the null hypothesis significance test can be obtained in Ioannidis (2019).

The ggplot graph has its axes constructed in such a way as to visualize a contrast between the theoretical quantiles of a distribution (in this case, the analysis is performed with the normal distribution) and the quantiles observed from the collected data set. The closer the points are to the 45º line, the closer the data distribution is to the distribution studied.

Tests on asymmetry and kurtosis values were chosen to analyze normality in all scans. By evaluating the kurtosis or flattening values, it is possible to measure the degree of tapering of the curve relative to the normal. Kurtosis measurements indicate the intensity of frequencies near the central values, approaching the mean with zero value. A leptokurtic curve indicates that most observed values approach the mean, indicating accurate data.

Due to the large number of points in the cloud of each plane, a calculation routine was developed to determine the statistics using MATLAB® R2015a Version 8.5.0.197613 software. The algorithm allowed reading text files in *.pts format, exported by the Faro Scene software, and the respective calculations and the generation of distribution curves and frequency histograms for the three axes.

3. Results and discussion

Once all scenes' processing and recording stage was completed, a point cloud was obtained for each flat face of the calibration part, where the values observed for the X, Y, and Z coordinates in each cloud approached the zero value. Thus, the variations of the observed values about the zero-reference value were considered errors attributed to the equipment, allowing an evaluation using descriptive statistics for each point cloud.

Tables 7 to 13 present the results obtained according to the scanning distance and the different resolutions, where the number of observations refers to the number used after eliminating outliers.

Table 7 – Statistics (in mm) obtained for scans performed at 1 meter.

Statistics	Resolution 1/2			Resolution 1/5			Resolution 1/8		
	X axis	Y axis	Z axis	X axis	Y axis	Z axis	X axis	Y axis	Z axis
Mean	0.0610	-0.0205	0.5410	0.0800	-0.0183	0.4837	0.1153	0.0084	0.5014
Std Deviation	1.8209	1.5338	2.3001	1.8175	1.4587	2.3139	1.7647	1.4770	2.3137
Variance	3.3158	2.3525	5.2903	3.3034	2.1277	5.3542	3.1141	2.1814	5.3532
Maximum	5.5000	4.5000	7.4000	5.5000	4.3000	7.4000	5.4000	4.4000	7.4000
Minimum	-5.4000	-4.6000	-6.3000	-5.3000	-4.3000	-6.4000	-5.1000	-4.4000	-6.4000
Mode	0.1000	-0.1000	0.9000	0.5000	-0.2000	0.8000	0.4000	0.0000	0.5000
Median	0.1000	0.0000	0.6000	0.1000	0.0000	0.6000	0.2000	0.0000	0.6000
Kurtosis	2.7192	2.8522	2.9875	2.6210	2.9022	3.1827	2.6488	2.8734	3.1126
Skewness	-0.1070	0.0176	-0.2003	-0.1233	0.0761	-0.1402	-0.1006	0.0545	-0.0889
Range	10.9000	9.1000	13.7000	10.8000	8.6000	13.8000	10.5000	8.8000	13.8000
RMS	1.8219	1.5339	2.3628	1.8193	1.4588	2.3639	1.7684	1.4769	2.3674
Observations	401080	247330	409810	63724	39915	67103	24587	15304	25697
Discarded	667	875	3318	103	216	763	23	65	212

Source: Authors (2024).

For scans performed at the shortest distance (1 meter), it is observed that the change in scanning resolution, where lower resolutions reduce the total number of observations, did not significantly impact the standard deviation value obtained. The averages were very close to the actual value (zero), and the standard deviations and RMS for the x and y

axes were less than 2 mm (nominal precision of the TLS FS80), presenting a slightly higher value for the z-axis. A more significant occurrence of outliers for the z-axis in the three resolutions tested is also worth noting.

The results for the scanning distance of 3 meters are presented in Table 8.

Table 8 – Statistics (in mm) obtained for scans performed at 3 meters.

Statistics	Resolution 1/2			Resolution 1/5			Resolution 1/8		
	X axis	Y axis	Z axis	X axis	Y axis	Z axis	X axis	Y axis	Z axis
Mean	0.0333	0.0289	0.1325	-0.0045	0.0408	0.1803	0.0382	-0.0039	0.1395
Std Deviation	1.8398	1.8964	2.1666	1.8622	1.8708	2.2077	1.8458	1.8403	2.4492
Variance	3.3847	3.5963	4.6940	3.4677	3.4999	4.8739	3.4068	3.3868	5.9986
Maximum	5.5000	5.7000	6.6000	5.5000	5.6000	6.4000	5.5000	5.5000	7.1000
Minimum	-5.4000	-5.6000	-6.3000	-5.4000	-5.5000	-6.2000	-5.4000	-5.5000	-7.2000
Mode	-0.3000	-0.2000	0.9000	-0.3000	0.2000	0.5000	-0.1000	0.1000	0.0000
Median	0.0000	0.0000	0.2000	-0.1000	0.0000	0.3000	0.0000	0.0000	0.2000
Kurtosis	2.7698	2.7547	2.4672	2.7686	2.7516	2.5445	2.8434	2.8038	2.4669
Skewness	0.1164	0.0712	-0.1397	0.1250	0.0571	-0.1297	0.1541	0.1196	-0.0924
Range	10.9000	11.3000	12.9000	10.9000	11.1000	12.6000	10.9000	11.0000	14.3000
RMS	1.8401	1.8966	2.1706	1.8621	1.8712	2.2149	1.8460	1.8402	2.4529
Observations	111660	92882	64327	17427	14867	9884	6768	5662	3717
Discarded	267	183	26	39	37	10	12	19	1

Source: Authors (2024).

At this distance, the results obtained for the standard deviations were like the scans at 1 meter. Still, there was a more excellent approximation of the z-axis averages to the actual value (zero) and a lower occurrence of outliers on this axis. It is worth mentioning that the scanning distance impacts the angle of incidence of the laser beam on the calibration piece. In contrast, for the z-axis, the vertical angles are closer to the nadir, and the distance to the calibration piece is more minor. Suppose there are systematic errors in the axis system and the vertical angular system of the TLS. In that case, the variations in this direction will be more evident, and the improvement is observed with the increase in distance. On the other hand, very long distances will impact the angle of incidence on the calibration piece (moving it away from perpendicularity), deteriorating the accuracy, as can be seen in the results for the distance of 25 meters.

Next, Table 9 shows the results obtained for the distance of 5 meters.

Table 9 – Statistics (in mm) obtained for scans performed at 5 meters.

Statistics	Resolution 1/2			Resolution 1/5			Resolution 1/8		
	X axis	Y axis	Z axis	X axis	Y axis	Z axis	X axis	Y axis	Z axis
Mean	-0.0097	0.0014	0.2241	-0.0093	0.0941	-0.1193	-0.0447	0.0125	0.0033
Std Deviation	1.7442	1.9063	2.4618	1.6886	1.9230	2.7248	1.7713	1.9641	2.9805
Variance	3.0421	3.6342	6.0606	2.8514	3.6980	7.4246	3.1375	3.8579	8.8836
Maximum	5.2000	5.7000	7.6000	5.0000	5.8000	7.7000	5.0000	5.9000	7.5000
Minimum	-5.2000	-5.7000	-7.1000	-5.0000	-5.6000	-7.9000	-5.3000	-5.8000	-8.6000
Mode	-0.4000	-0.1000	-0.2000	0.4000	0.4000	-1.6000	-0.5000	-0.8000	1.6000
Median	0.0000	0.0000	0.1000	0.0000	0.1000	-0.3000	0.0000	0.0000	0.1000
Kurtosis	2.8134	2.6938	2.6115	2.7961	2.6485	2.5819	2.8484	2.7198	2.5695
Skewness	0.0066	-0.0199	0.0777	0.0345	-0.0395	0.1630	-0.0852	-0.0015	-0.0190
Range	10.4000	11.4000	14.7000	10.0000	11.4000	15.6000	10.3000	11.7000	16.1000
RMS	1.7442	1.9063	2.4719	1.6885	1.9252	2.7270	1.7716	1.9638	2.9791
Observations	47362	42449	18292	7395	6804	2856	2930	2575	1047
Discarded	173	67	21	30	7	6	23	10	2

Source: Authors (2024).

At this distance, the results obtained for the standard deviations were like the scans at 1 and 5 meters away, maintaining a low number of outliers. However, with the increase in distance and a lower TLS resolution, a deterioration in the precision

of the z-axis was observed in the scan with a resolution of 1/8. In this case, the standard deviation increased to close to 3 mm. This effect of the decrease in resolution is reflected in the total number of points on the plane, which, added to the effects discussed in the previous distances for the z-axis, shows a degradation of the standard deviation on this axis with the decrease in resolution, going from 2.46 mm for the resolution of 1/2, going to 2.72 mm for the resolution of 1/5, and reaching 2.98 mm for the resolution of 1/8. This behavior is also repeated for this axis in the two previous distances.

Below is Table 10, with the results for the 10-meter scanning distance.

Table 10 – Statistics (in mm) obtained for scans performed at 10 meters.

Statistics	Resolution 1/2			Resolution 1/5			Resolution 1/8		
	X axis	Y axis	Z axis	X axis	Y axis	Z axis	X axis	Y axis	Z axis
Mean	0.0121	0.0431	-0.3029	0.0764	0.2043	-0.3411	0.1862	0.1949	-0.2800
Std Deviation	2.2526	2.4786	2.8682	2.4310	2.4951	3.7908	2.5338	2.6352	4.8475
Variance	5.0741	6.1436	8.2267	5.9099	6.2255	14.3700	6.4203	6.9444	23.4990
Maximum	6.7000	7.4000	8.3000	7.1000	7.5000	6.7000	7.5000	7.7000	8.7000
Minimum	-6.7000	-7.2000	-8.9000	-7.0000	-7.1000	-8.6000	-7.0000	-7.6000	-9.4000
Mode	-0.1000	0.2000	-1.8000	-0.5000	0.0000	-0.7000	-0.2000	-0.3000	-7.1000
Median	0.0000	0.1000	-0.5000	0.1000	0.2000	-0.4500	0.2000	0.1500	0.0000
Kurtosis	2.8447	2.8081	3.3747	2.7846	2.8752	2.1538	2.9602	2.9393	2.3901
Skewness	-0.0581	-0.0756	0.3941	0.0414	-0.0391	-0.0945	0.1072	0.1610	-0.1441
Range	13.4000	14.6000	17.2000	14.1000	14.6000	15.3000	14.5000	15.3000	18.1000
RMS	2.2525	2.4789	2.8835	2.4316	2.5027	3.7892	2.5391	2.6405	4.7331
Observations	13056	11896	2133	2075	1777	112	798	700	20
Discarded	45	40	40	97	31	0	16	33	0

Source: Authors (2024).

As the scanning distance increases to 10 meters, the results begin to be affected by the scanning distance. Note that the standard deviations for the x and y axes begin to reach values above 2 mm on all axes or that in the three previous scans, they were below 2 mm for the x and y axes. A few points stand out on the z-axis when using the 1/8 resolution. The manipulation on the z-axis becomes more significant because of the decrease in the incidence angle, with deviation values going from 2.87 mm for the 1/2 resolution to 3.79 mm for the 1/5 resolution and reaching 4.85 mm for the 1/8 resolution. The average values, however, remain very close to zero.

Since the number of points, especially on the z-axis, became very small as the scanning distance increased, it was decided to perform the experiments at distances of 15, 20, and 25 meters with resolutions of 1/1, 1/2, and 1/4, maintaining the resolution of 1/2 for all distances for a general analysis. At resolutions of 1/5 and 1/8, there were not enough points on all faces, making it impossible to generate the planes necessary for processing and registering the point cloud in the new reference.

It is also worth noting the change in the position of the calibration piece, placed at an inclination angle of 45º, which allowed for minimizing the problem of the incidence angle of the laser beam, thus increasing the number of points for the z-axis. The results obtained for the distance of 15 meters for the three proposed resolutions are presented in Table 11.

Table 11 – Statistics (in mm) obtained for scans performed at 15 meters.

Statistics	Resolution 1/1			Resolution 1/2			Resolution 1/4		
	X axis	Y axis	Z axis	X axis	Y axis	Z axis	X axis	Y axis	Z axis
Mean	0.0252	0.2247	-0.0400	-0.2106	0.1968	-0.1243	-0.2874	0.2586	-0.3377
Std Deviation	2.4946	2.7111	3.0405	2.6773	2.7601	2.9086	2.0180	1.9434	2.3173
Variance	6.2231	7.3502	9.2445	7.1680	7.6180	8.4601	4.0725	3.7766	5.3699
Maximum	7.3000	8.3000	9.0000	7.8000	8.4000	8.3000	5.0000	5.5000	5.9000
Minimum	-7.4000	-7.9000	-9.1000	-8.1000	-8.0000	-8.8000	-6.2000	-5.5000	-6.8000
Mode	0.2000	1.1000	1.0000	0.3000	-1.1000	-0.3000	-0.1000	-0.5000	0.4000
Median	0.1000	0.3000	0.1000	-0.1000	0.3000	0.0000	-0.1000	0.3000	-0.2000
Kurtosis	2.8469	2.8731	2.7533	2.8702	2.9049	2.8051	2.9043	2.8608	2.6401
Skewness	-0.1095	-0.1625	-0.1721	-0.1113	-0.0969	-0.1807	-0.2764	-0.1576	-0.2413
Range	14.7000	16.2000	18.1000	15.9000	16.4000	17.1000	11.2000	11.0000	12.7000
RMS	2.4947	2.7204	3.0407	2.6853	2.7668	2.9110	2.0375	1.9597	2.3408
Observations	19826	22186	21201	4351	5257	5213	1130	1267	1190
Discarded	77	95	33	21	10	22	7	3	1

Source: Authors (2024).

In the first analysis, the most significant number of points on the z-axis stands out after the part specification. At 10 meters at 1/2 resolution, the total number of points (used + outliers) was 2173; even increasing the distance to 15 meters, this number increased to 5235.

When evaluating the standard deviation values for the 1/2 resolution, slightly lower precision is observed on the three axes when compared to the 10-meter distance, reflecting the degradation due to the increase in distance. However, with the tilt of the part, an improvement in precision is observed on the three axes when the resolution is reduced from 1/1 to 1/4. Observing the practices recommended by the manufacturer FARO of the TLS FS80 model, it is highlighted that the resolution of 1/4 is recommended as the distance increases, as evidenced in this experiment's results (FARO, 2024).

For the distance of 20 meters, the results are presented in Table 12.

Table 12 – Statistics (in mm) obtained for scans performed at 20 meters.

Statistics	Resolution 1/1			Resolution 1/2			Resolution 1/4		
	X axis	Y axis	Z axis	X axis	Y axis	Z axis	X axis	Y axis	Z axis
Mean	-0.1261	0.2769	-0.0337	-0.2620	0.1569	0.0921	-0.0553	0.1614	0.3015
Std Deviation	3.4873	3.6630	4.1338	3.5466	3.7504	4.2001	2.8314	2.7008	3.4854
Variance	12.1610	13.4170	17.0880	12.5780	14.0660	17.6410	8.0168	7.2944	12.1480
Maximum	10.3000	11.2000	12.3000	10.0000	11.4000	12.2000	8.3000	7.2000	10.4000
Minimum	-10.5000	-10.7000	-11.8000	-10.7000	-11.0000	-11.1000	-7.7000	-7.8000	-8.7000
Mode	-0.4000	-0.7000	0.3000	0.2000	-1.5000	-1.1000	-2.1000	0.7000	0.5000
Median	-0.2000	0.2000	-0.1000	-0.2000	0.2000	0.0000	-0.2000	0.0000	0.4000
Kurtosis	2.7721	2.7913	2.6970	2.8031	2.8437	2.6027	2.9818	2.7588	2.4193
Skewness	0.0369	0.0113	0.0633	-0.0615	-0.0002	0.0652	0.3019	0.0709	-0.0816
Range	20.8000	21.9000	24.1000	20.7000	22.4000	23.3000	16.0000	15.0000	19.1000
RMS	3.4894	3.6733	4.1338	3.5555	3.7531	4.2003	2.8297	2.7035	3.4958
Observations	10442	11549	12197	2389	2840	2756	636	629	662
Discarded	17	29	25	10	2	4	1	13	3

Source: Authors (2024).

The standard deviation values increase significantly by increasing the distance to 20 meters, approaching values close to 4 mm at 1/1 and 1/2 resolutions but considerably lower at 1/4 resolution.

The results for the distance of 25 meters are presented in Table 13.

Table 13 – Statistics (in mm) obtained for scans performed at 25 meters.

Statistics	Resolution 1/1			Resolution 1/2			Resolution 1/4		
	X axis	Y axis	Z axis	X axis	Y axis	Z axis	X axis	Y axis	Z axis
Mean	-0.1389	0.0415	0.0182	0.2442	0.3890	0.1622	0.1026	0.3170	0.2027
Std Deviation	3.6974	3.8923	4.1725	3.7944	3.9888	4.1258	2.6669	2.7295	3.0995
Variance	13.6710	15.1500	17.4100	14.3970	15.9100	17.0220	7.1123	7.4500	9.6071
Maximum	10.8000	11.6000	12.5000	11.2000	11.5000	12.5000	7.0000	7.4000	7.6000
Minimum	-11.0000	-11.6000	-12.2000	-10.4000	-11.4000	-12.2000	-7.1000	-7.1000	-8.7000
Mode	1.2000	-1.2000	-0.5000	-0.8000	-1.3000	0.6000	-0.6000	0.4000	-2.3000
Median	-0.1000	0.1000	0.0000	0.3000	0.4000	0.1000	0.0000	0.4000	0.3000
Kurtosis	2.7967	2.8244	2.8069	2.7434	2.8840	3.0665	2.6503	2.9958	2.7655
Skewness	-0.0559	-0.0530	0.0155	-0.0245	-0.0463	0.0120	0.0244	-0.2056	-0.2322
Range	21.8000	23.2000	24.7000	21.6000	22.9000	24.7000	14.1000	14.5000	16.3000
RMS	3.6997	3.8922	4.1723	3.8011	4.0065	4.1278	2.6654	2.7446	3.1020
Observations	6727	7154	7272	1666	1665	1784	384	429	369
Discarded	31	48	16	6	11	0	2	17	0

Source: Authors (2024).

Finally, slightly higher values are observed for the standard deviations compared to the previous distance of 20 meters, maintaining the improvement pattern at the 1/4 resolution. With all the sample standard deviation values for each scanning distance and each resolution, aiming at a visual representation of what was discussed in the results of the previous tables, some graphs were generated for the three axes x, y, and z, showing the variation of the values obtained for each axis as a function of the scanning distance, as shown in Figures 9, 10 and 11.

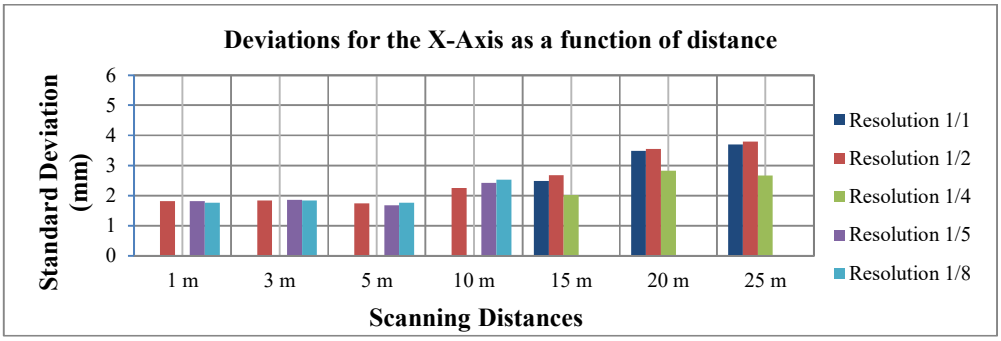

Figure 9 – Standard deviations obtained for the X-axis in the different scans.
Source: Authors (2024).

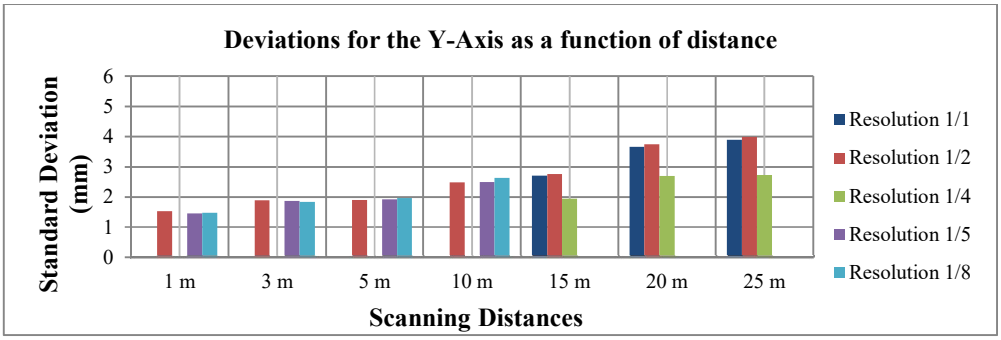

Figure 10 – Standard deviations obtained for the Y-axis in the different scans.
Source: Authors (2024).

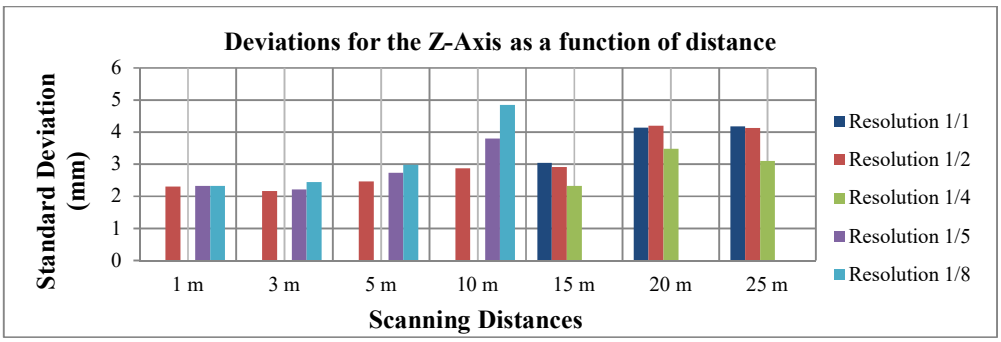

Figure 11 – Standard deviations obtained for the Z-axis in the different scans.
Source: Authors (2024).

After analyzing the deviations for the three axes, it was observed that the calibration proposal based on the 3D perpendicular plane system proved efficient and presented results consistent with the manufacturer's specifications. At short distances of 1, 3, and 5 meters, the standard deviations for the x and y axes were slightly smaller than the manufacturer's nominal error specification of 2 mm. On the z-axis, at these distances, the deviations were between 2 and 3 mm. The deviations were degraded for the distance of 10 meters, presenting values between 3 and 5 mm. By changing the inclination of the part and using the best resolutions, there was an improvement in precision, mainly at the 1/4 resolution with scanning at 15 meters. A degradation in precision was also observed as the distances increased to 20 and 25 meters.

Standard distribution curves, frequency histograms, and ggplot graphs were calculated for all scans to analyze the data's normality. However, for the sake of brevity, only the graphs obtained for the 1/2 resolution, which was used for all distances, are presented here.

Figures 12 and 13 show the standard distribution curves obtained for the three axes at distances from 1 to 25 meters.

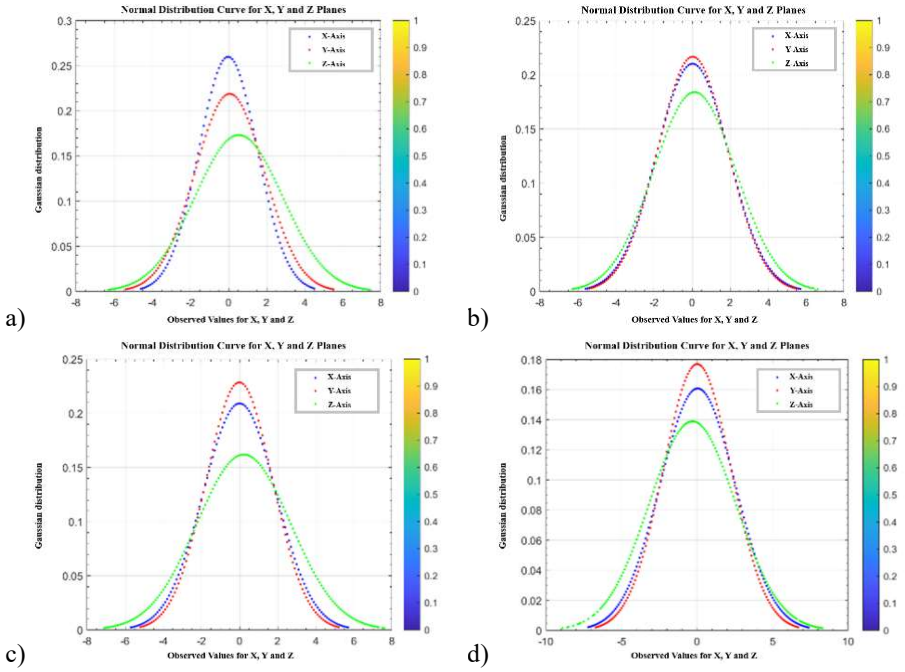

Figure 12 – Normal distribution curve obtained for the three axes: a) 1-meter scan with 1/2 resolution; b) 3-meter scan with 1/2 resolution; c) 5-meter scan with 1/2 resolution; and d) 10-meter scan with 1/2 resolution.
Source: Authors (2024).

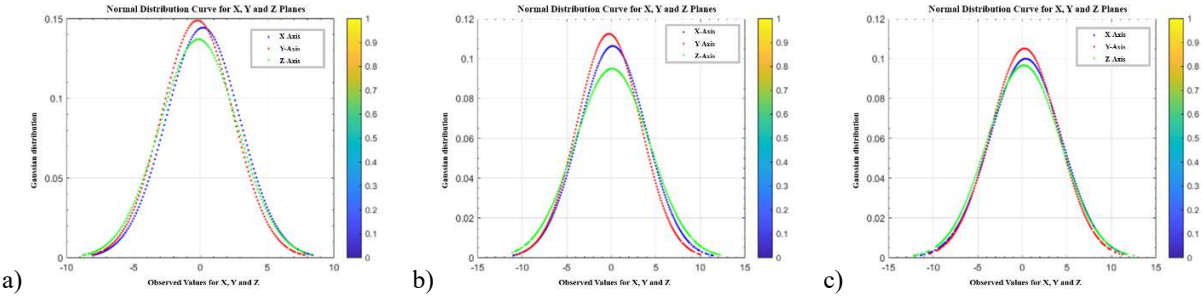

a) b) c)

Figure 13 – Normal distribution curve obtained for the three axes: a) 15-meter scan with 1/2 resolution; b) 20-meter scan with 1/2 resolution; and c) 25-meter scan with 1/2 resolution.
Source: Authors (2024).

Figures 14 and 15 show the graphs of the frequency histograms, and Ggplot obtained for scanning at 1 meter with a resolution of 1/2.

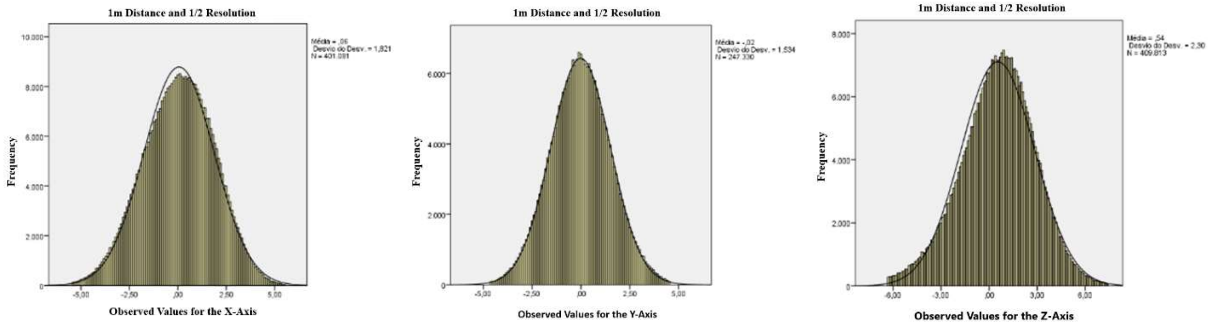

Figure 14 – Frequency histograms obtained for the three axes in scans performed at 1 meter with a resolution of 1/2.
Source: Authors (2024).

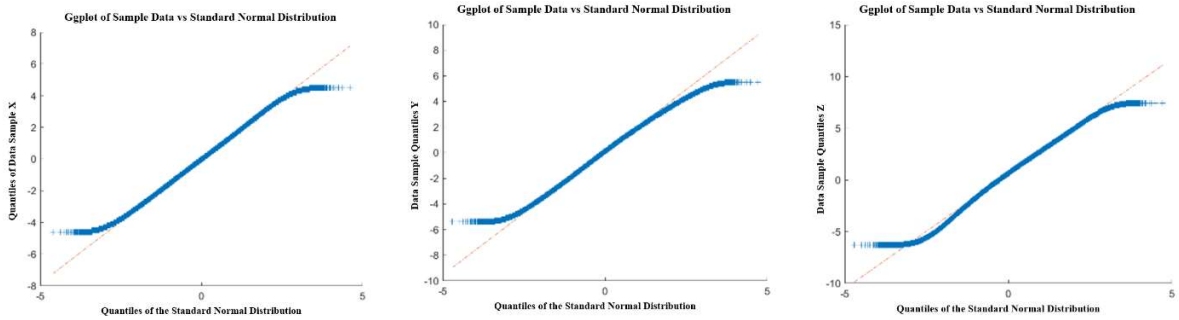

Figure 15 – Ggplot graphs obtained for the three axes in scans performed at 1 meter with a resolution of 1/2.
Source: Authors (2024).

Figures 16 and 17 show the graphs of the frequency histograms, and Ggplot obtained for the 25-meter scan with a resolution of 1/2.

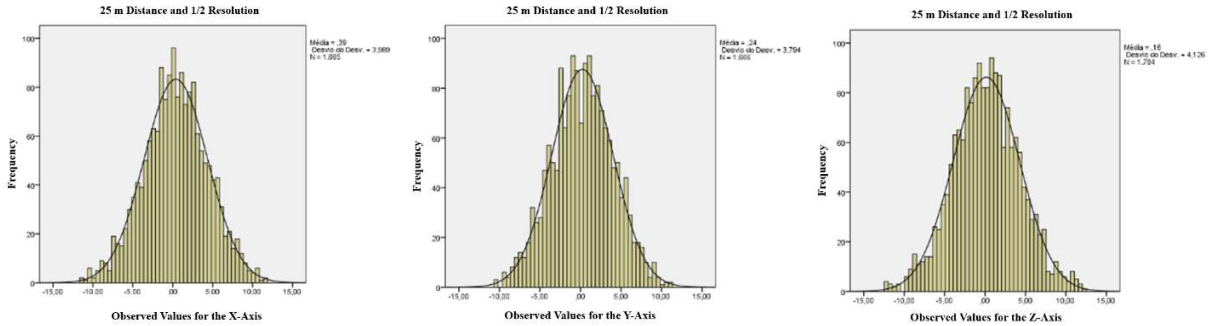

Figure 16 – Frequency histograms obtained for the three axes in scans performed at 25 meters with a resolution of 1/2. Source: Authors (2024).

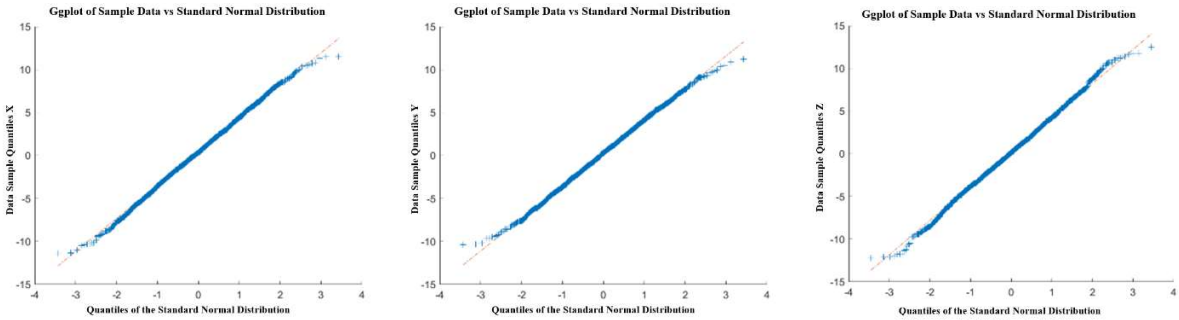

Figure 17 – Ggplot graphs obtained for the three axes in scans performed at 25 meters with a resolution of 1/2. Source: Authors (2024).

By analyzing the Ggplot graphs, most observed values show behavior related to a normal distribution, indicating strong evidence that the residuals are normal. Evaluating the quantile-quantile plot graphs obtained from the different clouds, most of them show favorable behavior with evidence of reference to a normal distribution. Only for the Z axis is it possible to notice, in some cases, that scans obtained at distances of 15, 20, and 25 meters have a leakage at the extremes. This behavior suggests the possibility of a mixture of distributions, which can also be observed from the analysis of the frequency histograms.

After the visual analysis, it was decided to present an analysis of the normality of the data based on isolated tests on the values of asymmetry (Sk) and kurtosis (K) for all scans. According to Ramos (1999), the values of asymmetry within the range "$-0.5 \leq Sk \leq 0.5$" and of kurtosis between the limits "$2.5 \leq K \leq 3.5$" can be used as an indication that the sample data follow a normal distribution.

After this analysis, Table 14 was obtained with the results for the different samples:

Table 14 – Assessment of skewness and kurtosis values for the different samples.

Scans	Skewness (-0.5 < Sk < 0.5)			Kurtosis (2.5 < K < 3.5)		
	X-Axis	Y-Axis	Z-Axis	X-Axis	Y-Axis	Z-Axis
Dist. 1m - Resolution 1/2	-0.11	0.02	-0.20	2.72	2.85	2.99
Dist. 1m - Resolution 1/5	-0.12	0.08	-0.14	2.62	2.90	3.18
Dist. 1m - Resolution 1/8	-0.10	0.05	-0.09	2.65	2.87	3.11
Dist. 3m - Resolution 1/2	0.12	0.07	-0.14	2.77	2.75	2.47
Dist. 3m - Resolution 1/5	0.12	0.06	-0.13	2.77	2.75	2.54
Dist. 3m - Resolution 1/8	0.15	0.12	-0.09	2.84	2.80	2.47
Dist. 5m - Resolution 1/2	0.01	-0.02	0.08	2.81	2.69	2.61
Dist. 5m - Resolution 1/5	0.03	-0.04	0.16	2.80	2.65	2.58
Dist. 5m - Resolution 1/8	-0.09	0.00	-0.02	2.85	2.72	2.57
Dist. 10m - Resolution 1/2	-0.06	-0.08	0.39	2.84	2.81	3.37
Dist. 10m - Resolution 1/5	0.04	-0.04	-0.09	2.78	2.88	2.15
Dist. 10m - Resolution 1/8	0.11	0.16	-0.14	2.96	2.94	2.39
Dist. 15m - Resolution 1/1	-0.11	-0.16	-0.17	2.85	2.87	2.75
Dist. 15m - Resolution 1/2	-0.11	-0.10	-0.18	2.87	2.90	2.81
Dist. 15m - Resolution 1/4	-0.28	-0.16	-0.24	2.90	2.86	2.64
Dist. 20m - Resolution 1/1	0.04	0.01	0.06	2.77	2.79	2.70
Dist. 20m - Resolution 1/2	-0.06	0.00	0.07	2.80	2.84	2.60
Dist. 20m - Resolution 1/4	0.30	0.07	-0.08	2.98	2.76	2.42
Dist. 25m - Resolution 1/1	-0.06	-0.05	0.02	2.80	2.82	2.81
Dist. 25m - Resolution 1/2	-0.02	-0.05	0.01	2.74	2.88	3.07
Dist. 25m - Resolution 1/4	0.02	-0.21	-0.23	2.65	3.00	2.77

Source: Authors (2024).

With the asymmetry analysis, it is possible to verify that the data collected for all samples behave related to a symmetrical distribution, considering the established limits.

From the analysis of the kurtosis values, a more significant flattening is observed on the Z axis, indicating a more excellent dispersion of the values observed around the mean, also verified from the analysis of the deviations found for this axis. Thus, it can be stated that the data used present a typical pattern for all scans on the x and y axes. For the z-axis, there is an indication of the presence of systematic errors in the observations for the following scans: distance of 3 meters and resolutions of 1/2 and 1/8; distance of 10 meters and resolutions of 1/5 and 1/8; and distance of 20 meters and resolutions of 1/4. The graph in Figure 11 shows that the more significant standard deviation on the z-axis is evident for the distances and resolutions mentioned. For the distance of 3 meters, the values were very close to the lower limit for kurtosis, presenting a calculated value of 2.47.

4. Final considerations

The proposed methodology proved efficient and presented results consistent with the expected errors according to the manufacturer's specifications. A determining factor in the point cloud's accuracy refers to the laser beam's incidence on the planes during scanning, where very acute incidence angles greatly influence the results, especially in the number of scan points. This influence can be observed by analyzing the deviations in the Z axis for distances from 1 to 25 meters at 1/2 resolution, used in all scans.

The proposal to adapt the positioning of the 3D part managed to obtain overwhelming and reliable results. It is also worth noting that manipulating the TLS performance reduces the resolution for distances of up to 10 meters and provides a better solution at 1/4 resolution for distances of 15, 20, and 25 meters.

The results prove the proposed methodology's efficiency, applied in laboratory shortage procedures using scans on short-range equipment, with the advantage of being an easy-to-implement method with fast results.

Acknowledgments

The authors would like to thank the Laboratory of Topography and Geodesy of the Department of Transportation Engineering of the Polytechnic School of USP for providing the space for the execution of the experiments; the company Alezi Teodolini for the loan of the Terrestrial Laser Scanner used in the experiment; and the CNPq for partial support with productivity grant PQ2 no. 402393/2009-0 for the manufacture of the calibration piece.

References

BOEHLER, W.; BORDAS, V.; MARBS, A., 2003. *Investigating Laser Scanner Accuracy*. The International Archives of Photogrammetry, Remote Sensing and Spatial Information Sciences. Vol. XXXIV, part 5/C15, pp696-701. Antalya.

CHOW, J. C. K., LICHTI, D.D., TESKEY, W. F., 2010. *Self-calibration of the TRIMBLE (MENSI) GS200 terrestrial laser scanner*. International Archives of Photogrammetry, Remote Sensing and Spatial Information Sciences, Vol. XXXVIII, Part 5 Commission V Symposium, Newcastle upon Tyne, UK, 161-166.

FARO, 2022. *Documentação de Usuário: FARO Focus Premium e FARO Focus Core*, p 138. FARO© Technologies Incorporation, October 2022. Available at: https://downloads.faro.com/index.php/s/CokPPexPAr7GeG8?dir=undefined&openfile=160759

FARO, 2024. *Documentação de Usuário: Práticas recomendadas para o Laser Scanner*, p. 11 e 12. FARO© Technologies Incorporation, May 2024. Available at: https://pt-knowledge.faro.com/Hardware/Focus/Focus/Laser_Scanner_Best_Practices.

HANCOCK, J. A., 1999. Laser Intensity-Based Obstacle Detection and Tracking. PhD thesis, The Robotics Institute, Carnegie Mellon University, Pittsburg, Pennsylvania.

HOLST, C.; NEUNER, H.; WIESER, A.; WUNDERLICH, T.; KUHLMANN, H. *Calibration of Terrestrial Laser Scanners*. Fachbeitrage begutachtet, pp. 147-157, 2016.

IOANNIDIS, J. P. A. What Have We (Not) Learnt from Millions of Scientific Papers with P Values? The American Statistician, 73(sup1), 2019, p. 20–25. DOI: https://doi.org/10.1080/00031305.2018.1447512

JORGENSEN, P. C., KUBIK, K., FREDERIKSEN, P.; WENG, W. Ah, robust estimation. Australian Journal of Geodesy, Photogrammetry and Surveying, No. 42, 1985, p. 19 – 32.

KERSTEN, Th., STERNBERG, H. and MECHELKE, K., 2005. *Investigations into the accuracy behavior of the terrestrial laser scanning system MENSI GS 100*. In Optical 3-D Measurement Techniques VII, A. Grün / H. Kahmen (Eds.), pp. 122 – 131.

KAASALAINEN, S., KROOKS, A., KUKKO, A., KAARTINEN, H., 2009. *Radiometric calibration of terrestrial laser scanners with external reference targets*. Remote Sens. 2009, 1, 144–158.

KUBIK, K., WENG, P.; FREDERIKSEN, P. Oh, grosserorors! Australian Journal of Geodesy, Photogrammetry and Surveying, No. 42, 1985, pp. 1 – 18.

LICHTI, D.D., 2007. Error modeling, calibration, and analysis of an AM-CW terrestrial laser scanner system. ISPRS Journal of Photogrammetry and Remote Sensing 61, 307-324.

LICHTI, D.D., 2008. A method to test differences between additional parameter sets with a case study in terrestrial laser scanner self-calibration stability analysis. ISPRS Journal of Photogrammetry and Remote Sensing 63, 169-180.

LICHTI, D.D., 2010. *Terrestrial laser scanner self-calibration: correlation sources and their mitigation*. ISPRS Journal of Photogrammetry and Remote Sensing 65, 93-102.

MEDIĆ, T.; KUHLMANN, H.; HOLST, C. (2021). Empirical Evaluation of Terrestrial Laser Scanner Calibration Strategies: Manufacturer-Based, Target-Based and Keypoint-Based. In: Kopáčik, A., Kyrinovič, P., Erdélyi, J., Paar, R., Marendić, A. (eds) Contributions to International Conferences on Engineering Surveying. Springer Proceedings in Earth and Environmental Sciences. Springer, Cham. https://doi.org/10.1007/978-3-030-51953-7_4

MIOT, H. A. Avaliação da normalidade dos dados em estudos clínicos e experimentais. Jornal Vascular Brasileiro, 16(2), 2017, p. 88-91. DOI: https://doi.org/10.1590/1677-5449.041117

QIANG, Z., WEI, W., 2009. *Calibration of laser scanning system based on a 2D ball plate. Measurement*, v. 42, 963-968. https://doi.org/10.1016/j.measurement.2009.02.004.

QIAO, J.; BUTT, J. A. *Self-calibration of terrestrial laser scanner using a M3C2-based planar patch algorithm*. ISPRS Journal of Photogrammetry and Remote Sensing, Volume 197, 2023, p. 335-345, ISSN 0924-2716. DOI: https://doi.org/10.1016/j.isprsjprs.2023.02.008.

RAMOS, A.W, 1999. *Uma contribuição aos estudos de capacidade de máquina*. Tese de Doutorado. Escola Politécnica. Universidade de São Paulo. São Paulo. 298p.

RESHETYUK, Y., 2006. *Investigation and calibration of pulsed time-of-flight terrestrial laser scanners*. Licentiate thesis in Geodesy. Royal Institute of Technology (KTH), Stockholm, Sweden.

RESHETYUK, Y., 2010. *A unified approach to self-calibration of terrestrial laser scanning*. ISPRS Journal of Photogrammetry and Remote Sensing 65, 445-456.

SHAN, J., TOTH, C.K. (Eds.)., 2017. *Topographic Laser Ranging and Scanning: Principles and Processing*, Second Edition (2nd ed.). CRC Press. https://doi.org/10.1201/9781315154381.

SOUDARISSANANE, S., LINDENBERGH, R., MENENTI, M., TEUNISSEN, P., 2011. *Scanning geometry: Influencing factor on the quality of terrestrial laser scanning points*. ISPRS Journal of Photogrammetry and Remote Sensing 66, 389-399.

SHI, S.; MURALIKRISHNAN, B.; SAWYER, D. Terrestrial laser scanner calibration and performance evaluation using the network method, Optics and Lasers in Engineering, Volume 134, 2020, 106298, ISSN 0143-8166. DOI: https://doi.org/10.1016/j.optlaseng.2020.106298.

TELLING, J.; LYDA, A.; HARTZELL, P.; GLENNIE, C., 2017. *Review of Earth science research using terrestrial laser scanning*. Earth-Science Reviews 169, 35-68. https://doi.org/10.1016/j.earscirev.2017.04.007

ZHOU, T.; CHENG, X.; LIN, P.; WU, Z.; LIU, E. A General Point-Based Method for Self-Calibration of Terrestrial Laser Scanners Considering Stochastic Information. Remote Sens. 2020, 12, 2923. https://doi.org/10.3390/rs12182923